A Feasibility Study on Burnable Absorber in a Long-Life Maritime Molten Salt Fast Reactor Using Chloride-Fluoride Hybrid Salt

Young-June Lee, Yonghee Kim*
Department of Nuclear & Quantum Engineering, Korea Advanced Institute of Science and Technology (KAIST), 291 Daehak-ro, Yuseong-gu, Daejeon 34141, Republic of Korea
**Corresponding author: yongheekim@kaist.ac.kr*

Keywords: Molten Salt Fast Reactor (MSFR), Burnable Absorber (BA), Chloride-Fluoride Hybrid Salt

1. Introduction

The Molten Salt Fast Reactor (MSFR) offers significant advantages for maritime applications, including unparalleled safety features due to the use of liquid salt fuel, which can potentially eliminate severe accidents. Unlimited integrity of liquid salt fuel maximizes the fuel utilization efficiency. Additionally, MSFRs do not require stringent online fuel management.

However, the low fissile density of salt fuel requires a large inventory, even with 19.75 wt.% HAELU. For maritime MSFRs with low thermal power (100 MWth), minimizing fuel inventory is crucial, achievable through a moderating reflector [1].

To address this challenge, Chloride-fluoride hybrid salt is a promising candidate due to its higher uranium density. One key benefit is the potential use of an MgO reflector, avoiding the costly BeO.

Even in MSFRs, burnable absorbers (BA) provide extremely simplified reactivity control mechanisms through a surgical moderation effect [1]. However, the hard neutron spectrum of the MgO reflector challenges the use of conventional BAs. Hence a feasibility study on BAs in long-life maritime MSFRs using chloride-fluoride hybrid salt has been conducted.

2. Conceptual Design of Maritime MSFR using a KCl-UCl_3-UF_4 Salt Fuel

2.1 Material and Neutronic Properties

Table I lists the properties of NaCl-KCl-UCl_3 and KCl-UCl_3-UF_4 at their eutectic compositions. It is evident that the uranium density of hybrid salt is 75% higher than that of the chloride salt with a similar eutectic melting temperature.

To minimize the required uranium inventory, 19.75 wt.% HALEU is used, and 99% enriched Cl-37 is employed to avoid parasitic capture by Cl-35. Equation (1) represents the temperature-dependent density of each individual salt component in the liquid state [2,3], while the liquid behavior of 28.0 KCl-36.0 UCl_3-36.0 UF_4 is described by the Ideal Liquid Model, as shown in Equation (2). The notations X_i, M_i, and V_i denote the mole fraction, molar mass, and molar volume of each fuel salt component. For a conservative estimate, the density of 28.0 KCl-36.0 UCl_3-36.0 UF_4 at the eutectic melting point is adjusted based on the solid-state density of each salt component using the Ideal Liquid Model. It is then assumed that the liquid behavior beyond the eutectic melting point follows the evaluated liquid properties.

Table II provides the material densities used in the calculations, including considerations for thermal expansion. The reactor is assumed to operate in a 900 K isothermal state, with the inlet and outlet temperatures of the active core corresponding to 590°C and 650°C, respectively.

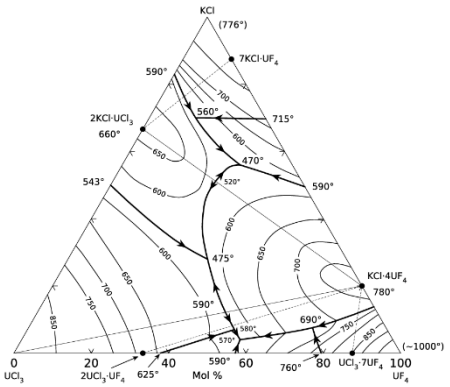

Fig. 1. Phase diagram of KCl-UCl_3-UF_4 [4].

Table I: Properties of NaCl-KCl-UCl_3 and KCl-UCl_3-UF_4

Fuel salt	NaCl-KCl-UCl_3	KCl-UCl_3-UF_4
Eutectic melting temperature	470.15 °C	475 °C
Mole fraction	42.9-20.3-36.8	28.0-36.0-36.0
Uranium density	1.702 g/cm^3	2.99 g/cm^3

$$\rho_i(T) = A_i - B_i \cdot T \; [g \cdot cm^{-3}] \quad (1)$$

$$\rho(T) = \frac{\sum X_i M_i}{\sum X_i V_i} \; [g \cdot cm^{-3}] \quad (2)$$

Table II: Material densities

Material	■ Inconel625	■ SS316	■ MgO
ρ [g/cm^3]	8.12	7.674	3.488
Material	■ KCl-UCl_3-UF_4	■ B_4C (Drum)	
ρ [g/cm^3]	4.543 (900 K)	2.4696	

Fig. 2 illustrates a simple cylindrical active core containing only salt fuel, with the black region indicating a vacuum. Fig. 3 shows the neutron multiplication as a function of diameter. At a diameter of approximately 170 cm, the reactor becomes critical with only salt fuel by

itself, due to its superior fissile density. This presents challenges for controlling excess reactivity or reactor shutdown, as the reactivity control devices are loaded in the reflector region.

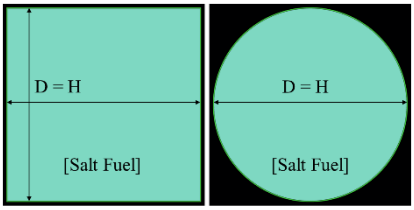

Fig. 2. Simple cylindrical shape of the active core

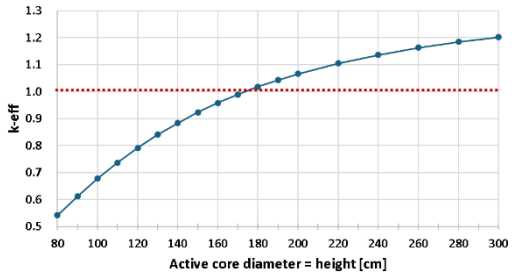

Fig. 3. K-eff of fuel salt as a function of the geometric size.

2.2 Reactor Model

Fig. 3 illustrates the simple cylindrical design of the maritime MSFR, which uses a 60 cm MgO reflector. The active core is enclosed by a 0.8 mm Inconel 625 cladding and an 8 mm SS316 inner barrier.

To select the optimal reflector material, BeO, MgO, and SS316 reflectors were evaluated. Only the size of the active core was adjusted to achieve 25 effective full power years (EFPY) at 100 MWth fission power, while the thickness of the reflector and inner barrier remained constant. The inactive salt volume was assumed to be identical to the active core volume. Depletion calculations were performed using the Monte Carlo code Serpent 2.2.1 with the ENDF/B-VII.1 cross-section library under 900 K conditions. The simulation used 100 inactive cycles, 300 active cycles, and 50,000 histories per cycle, resulting in an uncertainty of 15 pcm.

Figs. 4 and 5 show the k_{eff} and conversion ratio for the three reflectors. While BeO is inevitable for minimizing fuel inventory in the NaCl-KCl-UCl_3 MSFR [1], it is less effective with hybrid salt. MgO reflector, on the other hand, is more desirable for maintaining a favorable conversion ratio. Though it requires a slightly higher HALEU inventory, excluding the costly BeO is desirable.

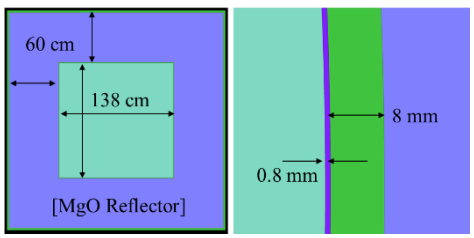

Fig. 3. Reactor configuration of MSFR using MgO reflector.

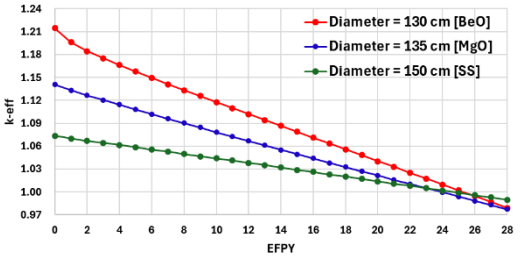

Fig. 4. K_{eff} profile of reactor candidates targeting 25 EFPY

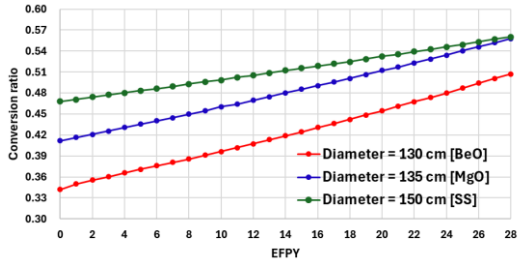

Fig. 5. Conversion ratio throughout the operation lifetime.

Table III: Fuel salt inventory of reactor candidates

Reflector	BeO	MgO	SS
Active core diameter [cm]	130	138	150
Active core volume [m^3]	1.73	2.06	2.65
Inactive salt volume [m^3]	1.73	2.06	2.65
HALEU inventory [t]	10.33	12.35	15.87
Burnup at 25 EFPY [MWD/KgU]	88.41	73.90	57.55

3. Application of Burnable Absorber

3.1 Rod and Pad-type BA

Since MgO is not an effective moderating reflector, controlling excess reactivity becomes difficult due to the hard neutron spectrum. This makes it challenging to utilize the self-shielding effect of burnable absorbers (BA) by adjusting their geometry, as shown in Fig. 6. Fig. 7 shows the depletion results for rod and pad-type B4C, which are attached to the radial surface of the inner barrier, with a height of 138 cm. A 60% theoretical density (TD) and natural abundance of boron were used to mitigate swelling caused by helium accumulation. While adjusting the self-shielding effect is an effective way to control excess reactivity with a BeO reflector, this concept is not feasible with the MgO reflector.

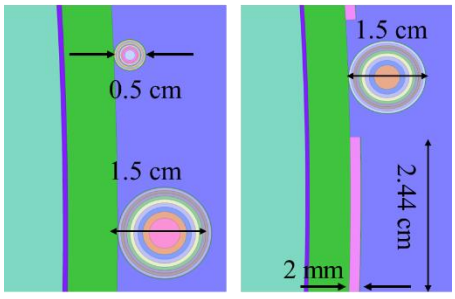

Fig. 6. Illustration of rod and pad type BA (Top View).

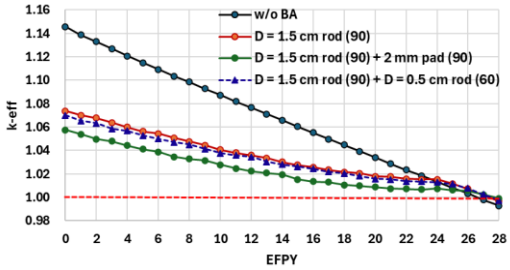

Fig. 7. Depletion results of rod and pad type BA.

3.2 Impurity-type BA

One alternative is to homogeneously dilute the BA material within the MgO reflector, as an impurity, as shown in Fig. 8. As the accumulation of helium in the reflector region is undesirable, the usage of gadolinium could be considered. Due to the impracticality of enriching Gd-155 and Gd-157, natural abundance gadolinium was used.

0.06 at% B-10 and 0.197 at% Gd, which consist of 0.06 at% of Gd-155 and Gd-157, were diluted in a 10 cm region, and the depletion results are shown in Fig. 9. While B-10 is effective at controlling excess reactivity and is fully burnable, there is a reactivity penalty of 2,000 pcm with Gd, even after the depletion of Gd-155 and Gd-157. This is because of the resonance capture reaction of the residual isotopes, especially Gd-156, as shown in Figs. 10 and 11, particularly in the epithermal neutron energy spectrum.

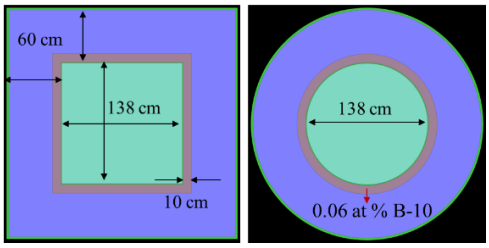

Fig. 8. Illustration of impurity type BA.

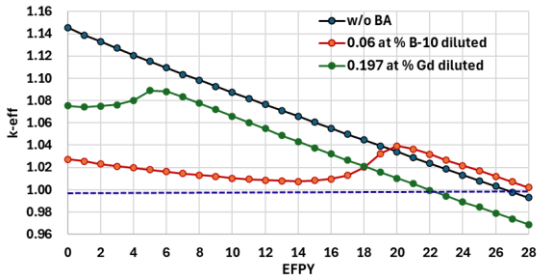

Fig. 9. Depletion results of impurity type BA.

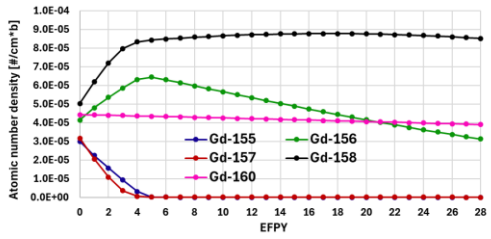

Fig. 10. Atomic number densities of Gd isotopes throughout the operation lifetime.

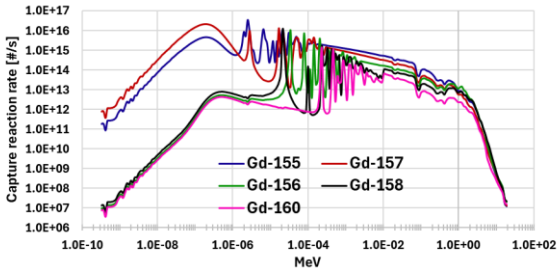

Fig. 11. 238 energy group-wise capture reaction rate of Gd isotopes at BOL (0 EFPY).

3.3 Simplification of BA

Since the self-shielding effect of B4C is not effective with the MgO reflector, a simpler shell-type B4C of 5.3 mm is attached to the radial surface of the inner barrier, with a 0.1 mm SS316 canning, as shown in Fig. 12. Additionally, two types of BA were evaluated at the top and bottom of the inner barrier: a 2 mm plate-type B4C with 0.1 mm SS316 canning and a 0.3 at% B-10 diluted MgO reflector of 10 cm, as shown in Fig. 13.

Fig. 14 shows the depletion results for both cases. In both cases, the reactivity fluctuates between 800 pcm and 2,000 pcm over the operational lifetime. The only discernable difference occurs between 10 and 14 EFPY, where the axial impurity-type BA depletes faster due to slightly weaker self-shielding.

Furthermore, the discretization of depletion regions, as shown in Figs. 12 and 13, hardly affects the depletion profile due to the weak self-shielding effect. In other words, it provides robustness against uncertainties in long-life nuclear designs, such as B_4C deformation due to swelling or dislocation.

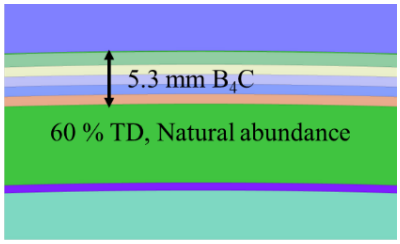

Fig. 12. Illustration of radial B_4C shell (Top View).

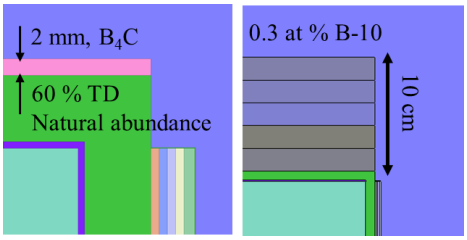

Fig. 13. Illustration of axial B_4C shell (left) and axial impurity type BA (right) (Side View).

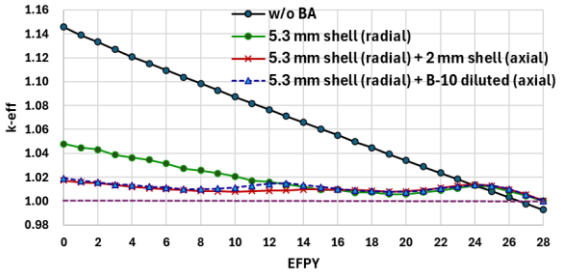

Fig. 14. Depletion results of simplified BAs.

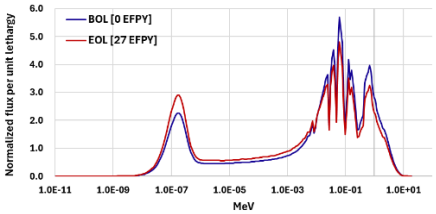

Fig. 15. Whole-core neutron energy spectrum with BA.

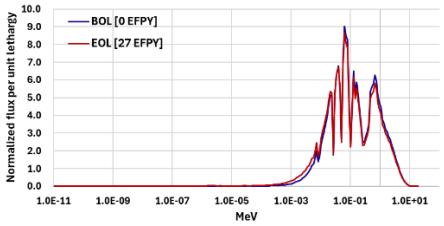

Fig. 16. Active core neutron energy spectrum with BA.

To control residual excess reactivity, seven control drums are placed in the MgO region, as shown in Fig. 17. The B4C thickness is 5 cm, and 90% enriched B-10 is used. The reactivity control drum is enclosed by 0.3 mm SS316 canning and a 0.7 mm SS316 guide tube, which mainly reduces the excess reactivity by loading the control drum. The effect of a relatively thick 1 mm SS316 canning for the B4C shell was also evaluated, as depicted in Fig. 18.

Fig. 19 shows the depletion results for the shell-type B_4C with reactivity control drums and 1 mm SS316 canning. At 27 EFPY, it is evident that the reactivity decrement due to the control drums and the 1 mm SS316 canning is minimal, owing to the hard neutron energy spectrum. However, the reactivity profile can be further refined by adjusting the B_4C shell thickness or appropriately managing fission product removal.

As summarized in Table IV, the reactor becomes subcritical in the drum-inward state at 0 EFPY. However, additional reactivity devices, such as shutdown plates, are needed to ensure an adequate shutdown margin.

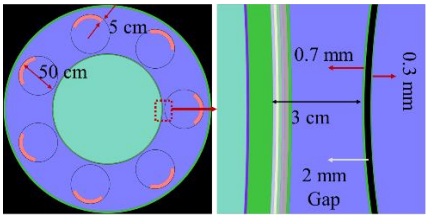

Fig. 17. Configuration of the reactivity control drums.

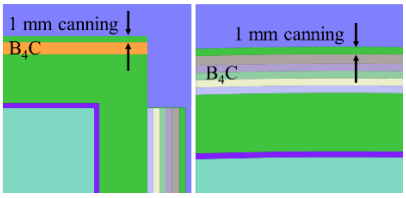

Fig. 18. Illustration of 1 mm SS316 canning.

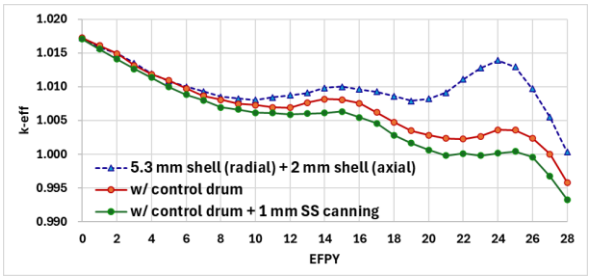

Fig. 19. Depletion profile with drum and 1mm SS canning.

Table IV: Control drum worth at BOL (0 EFPY)

Hot full power (900 K)	All drum outward	All drum inward	Drum worth
k_{eff}	1.01727	0.99439	2,274 pcm

4. Conclusions

The superior fissile density of hybrid salt enables the use of the MgO reflector in the maritime MSFR with a reasonable fuel inventory, based on favorable neutron economy, while excluding the costly BeO reflector.

However, the hard neutron energy spectrum presents a challenge in controlling excess reactivity using conventional rod or pad-type BAs. To address this, impurity-type BAs using B-10 and shell-type BAs utilizing B4C (60% TD and natural boron) were proposed. Both methods effectively suppress excess reactivity throughout the operational lifetime, with reasonable reactivity swings.

ACKNOWLEDGMENTS

This work was supported by the National Research Foundation of Korea(NRF) grant funded by the Korea government(MSIT) (RS-2023-00260898)

REFERENCES

[1] Youngjune Lee, Eunhyug Lee, and Yonghee Kim, “A Physics Study for an Innovative Long-life Small Molten Salt Fast Reactor (MSFR) for Ship Propulsion”American Nuclear Society. Transactions, 130, 1014-1017.
[2] Parker, Stephen Scott, et al. "Thermophysical properties of liquid chlorides from 600 to 1600 K: Melt point, enthalpy of fusion, and volumetric expansion." Journal of Molecular Liquids 346 (2022): 118147.
[3] W. M. Haynes, D. R. Lide, & T. J. Bruno (2016). CRC handbook of chemistry and physics. CRC press.
[4] Desyatnik, V. N., Katyshev, S. F., Raspopin, S. P., & Trifonov, I. I. (1973). Phase diagram of the KCl-UCl 3-UF 4 system. *Izvestiya Vysshikh Uchebnykh Zavedenij. Tsvetnaya Metallurgiya*, 132-134.